Karakalpak Scientific Journal

Volume 3
Issue 1 *Issue 1*

Article 25

3-3-2020

Long-term variations (2001-2016) of satellite-based PM2.5 concentrations and its determinants in Xinjiang, northwest of China

Wei Wang
University of Chinese Academy of Sciences

Alim Samat
Research Center for Ecology and Environment of Central Asia

Jilili Abuduwaili
State Key Laboratory of Desert and Oasis Ecology, jilil@ms.xjb.ac.cn

Long-term variations (2001-2016) of satellite-based $PM_{2.5}$ concentrations and its determinants in Xinjiang, northwest of China

Wei Wang[1,2,3], *Alim* Samat[1,2,] , and *Jilili* Abuduwaili[1,2,3]

[1]State Key Laboratory of Desert and Oasis Ecology, Xinjiang Institute of Ecology and Geography, Chinese Academy of Sciences 830011 Urumqi, China

[2] Research Center for Ecology and Environment of Central Asia, Chinese Academy of Sciences 830011 Urumqi, China

[3] University of Chinese Academy of Sciences, 100049 Beijing, China

Abstract. Based on the long-term series of satellite-retrieved $PM_{2.5}$ concentrations, this study explored the spatiotemporal variation and aggregation characteristics of $PM_{2.5}$ concentrations in Xinjiang from 2001 to 2016 by using standard deviational ellipse analysis and spatial autocorrelation statistics method. The result showed that the annual average $PM_{2.5}$ concentrations was high in the north slope of Tianshan mountain and the western Tarim desert where High-High clusters mainly distribute. Furthermore, $PM_{2.5}$ concentrations in the north slope of Tianshan mountain increased significantly from 2001 to 2016. Based on the result of GeoDetector model, population density was the most dominant factor of $PM_{2.5}$ concentrations (q=0.55). With the rapid urbanization and expansion of oasis, the driving force of population density on $PM_{2.5}$ concentrations are gradually decreasing. However, DEM, NSL, LCT and NDVI show the increased trend on the driving forces of $PM_{2.5}$ concentrations.

Key words: satellite-retrieved, concentration, variation, analysis.

1 Introduction

The atmospheric particulate matter with a diameter of 2.5 μm or less ($PM_{2.5}$) is the common indicator of air quality both indoor and outdoor. Most of $PM_{2.5}$ is emitted from power plants, industries, automobiles constructions sites, fires and so on. WHO estimates that 90% people worldwide breath air containing high levels of $PM_{2.5}$. Numerous epidemiological studies have shown that long-term $PM_{2.5}$ exposure can increase the incidence of cardiovascular and respiratory diseases, as well as lung cancer [1,2].

With the fast industrialization and urbanization process over the past three decades, atmospheric pollution is become a ubiquitous and serious problem in China. A growing number of researches have dedicated enormous efforts focused on $PM_{2.5}$ problems in eastern coastal China, such as Beijing, Tianjin, Hebei, Nanjing, Shanghai[3-5]. However, few studies explored the spatiotemporal variations of $PM_{2.5}$ constrictions and its driving factors in northwest of China, especially Xinjiang. In the northern part of the Tianshan Mountains and the western margin of the Tarim Basin, about 10 million people have suffered from serious air pollution in the past decade[6].

Xinjiang is the largest administrative region as well as the largest arid land in China which means less precipitation and vegetation distribution which has strong removal and absorption capacity for $PM_{2.5}$[7,8]. Thus, harsh climate and environment are more likely to cause accumulation of atmospheric pollutants. The spatial pattern and variations of $PM_{2.5}$ concentrations, especially spatial autocorrelation and heterogeneity, in arid land is worthy of study and discussion. Meanwhile, identifying the natural and socio-economic determinants of $PM_{2.5}$ concentrations contribute to effectively solve air pollution problems in this region. Therefore, the purposes of this study were (1) exploring the spatiotemporal characteristics of $PM_{2.5}$ concentrations by spatial autocorrelation analysis. (2) identifying the dominant factors responsible for spatiotemporal variations, especially the socio-economic factors. (3) quantitatively analysing the interannual variations of the dominant power of $PM_{2.5}$ driving factors.

2 Materials and Methods

1.1 Data Source

This study used the global annual mean surface $PM_{2.5}$ concentrations grids which estimated by Aerosol Optical Depth (AOD) retrievals from multiple satellite products (MISR, MODIS-DT, MODIS-DB, MODIS-MAIAC, and SeaWiFS-DB)[9]. The satellite based gridded $PM_{2.5}$ dataset has a spatial resolution of 0.01x0.01 degree, and it was combined with simulation (GEOS-Chem model) based on the ground photometer observations from 1998-2016. Other dataset and sources we used on this study shown in Table 1.

Table1 Data source

Dataset	Data Sources
Land Cover type (LCT)	MODIS MCD12Q1 (2001-2016) [10]
Albedo	MODIS MCD43A3 (2001-2016) [11]
Land Surface Temperature (LST)	MODIS MOD11A2 (2001-2016) [12]
Normalized Difference Vegetation Index (NDVI)	MODIS MOD13Q1 (2001-2016) [13]
Nighttime Stable Light (NSL)	National Geophysical Data Center DMSP-OLS (2001-2013) /NPP-VIIRS (2013-2016) [14,15]
Digital Elevation Model (DEM)	NASA Shuttle Radar Topographic Mission 90m [16]
Climate Zone (CZ)	Köppen-Geiger climate classification maps (2000-2015) [17]
Population Data (POP)	Asia Continental Population Dataset (2000, 2005, 2010, 2015, 2020) [18] and 2017 Xinjiang Statistical Year book
Gross Domestic Product in 2016(GDP)	2017 Xinjiang Statistical Year book
Industrial GDP 2016 (INGDP)	2017 Xinjiang Statistical Year book
Road Network Length in 2016 (Road_L)	OpenStreetMap historical dataset (https://www.openstreetmap.org/)
River Network Length in 2016 (River_L)	OpenStreetMap historical dataset (https://www.openstreetmap.org/)

2.2 Method

2.2.1 Standard deviational ellipse analysis

The standard deviational ellipse (SDE) analysis can delineates the geographical distribution trend of concerned features. SDE is calculated based on the average center of discrete points and the standard distance of other points away from the mean center. The calculated major and minor axes of the ellipse indicate the direction and data distribution range. Based on this, SDE also known as the directional distribution analysis. In this study, the spatial characteristics and the annual moving trace of $PM_{2.5}$ concentrations can revealed by the spatial extent, spatial orientation, spatial shape and spatial center of the standard deviational ellipse [19].

2.2.2 Spatial autocorrelation statistics

Spatial autocorrelation statistics included global spatial autocorrelation and local spatial autocorrelation. Based on the Tobler's First Law of Geography, Patrick Moran invented the global Moran's I which can examine the spatial autocorrelation patterns of $PM_{2.5}$ concentration [20]. The global Moran's I and Z_I-score was calculated as follows:

$$I=\frac{\mathrm{n}}{S_0}\frac{\sum_{i=1}^{n}\sum_{j=1}^{n}w_{i,j}z_iz_j}{\sum_{i=1}^{n}z_i^2} \quad (1)$$

$$Z_I=\frac{I-E[I]}{\sqrt{E[I^2]-E[I]^2}} \quad (2)$$

Where n is the number of sample regions, z_i is the deviation of an attribute for feature i from its mean (x_i-$\overline{X}$), $\overline{X}$ is the mean of corresponding attribute, $w_{i,j}$ is the spatial weight matrix; S_0 is the aggregate of all the spatial weights. *E[I]* is computed as -1/(n-1). The value of global Moran's I range from -1 to 1. The value less than 0, greater than 0, equal to 0 indicates negative correlation, positive correlation, no correlation, respectively. The reliability of Moran's I (existence of spatial autocorrelation) are tested by using the standardized statistic Z_I-score.

Local Indicators of Spatial Association (LISA) was introduced to interpret the local pockets of nonstationary and location of hot spots [21].It can also be used to assess the impact of individual region on the global statistics. Here we use local Moran's I which is computed as:

$$I_{\mathrm{i}}=\frac{x_i-\overline{X}}{S_i^2}\sum_{j=1,j\neq x}^{n}w_{i,j}\left(x_j-\overline{X}\right) \quad (3)$$

$$S_{\mathrm{i}}^2=\frac{\sum_{j=1,j\neq i}^{n}\left(x_j-\overline{X}\right)^2}{n-1}-\overline{X}^2 \quad (4)$$

Where x_i is an attribute for feature i, $\overline{X}$ and w_{ij} are the same as in Equ.(1).

2.2.3 GeoDetector model

Based on the spatially stratified heterogeneity, which refers to the phenomena that within strata are more similar than between strata, the fundamental theory of the GeoDetector model was first proposed by Wang, *et al.* [22]. The GeoDetector model applies q value to quantitatively measure the heterogeneity and autocorrelation of the dependent variable and detects the association between the dependent variable and its influencing factors.

$$q=1-\frac{\sum_{h=1}^{L}N_h\sigma_h^2}{N\sigma^2}$$

where N refers to the total number of sample units in the entire study area, and represents the global variance in Y in the entire study area. the study area was stratified into L zones (h=1, …, L), and the stratification depends on the characteristics of the explanatory variables or determinant factors (X). and represent the number of sample units and the variance in Y within zone h considering fact X, respectively. The model consists of the following four modules:

1) The factor detector calculates the determinant power of an explanatory variable X of Y.

2) The risk detector maps the average value of response variable in each strata.

3) The interaction detector can reveal the interactive influence of X1 and X2 on Y.

4) The ecological detector identifies the difference of the impacts between X1 and X2

3 Results

3.1 Spatiotemporal characteristics of $PM_{2.5}$ concentrations

Figure1 shows that the significant spatial differences of $PM_{2.5}$ concentrations exited in Xinjiang. $PM_{2.5}$ concentrations were higher in urban agglomeration which located in northern Tianshan and western Tarim Basin, especially in Shihezi(19.96μg/m3), Kashi(19.67μg/m3), Shule(18.09μg/m3), Yining(17.51μg/m3), Kuitun(17.42μg/m3), Dushanzi(16.50μg/m3). However, it was lower in sparsely-populated area in eastern and southern Xinjiang. Furthermore, an exception was found in northern Tianshan, where $PM_{2.5}$ concentrations was increased at an annual rate of 1.1-1.7μg/m3/yr. While in the southern Tianshan, $PM_{2.5}$ concentrations were decreased with the rates ranging from -0.1-0.7μg/m3/yr. Based on SDE analysis, Figure 2 shows that the main distribution of $PM_{2.5}$ concentrations was aligned in the southwest-northeast direction. And the median center made a clear but gradual shift from southwest to northeast. This movement mainly caused by rapid increase of the high $PM_{2.5}$ concentrations in the northern slope of Tianshan Mountain.

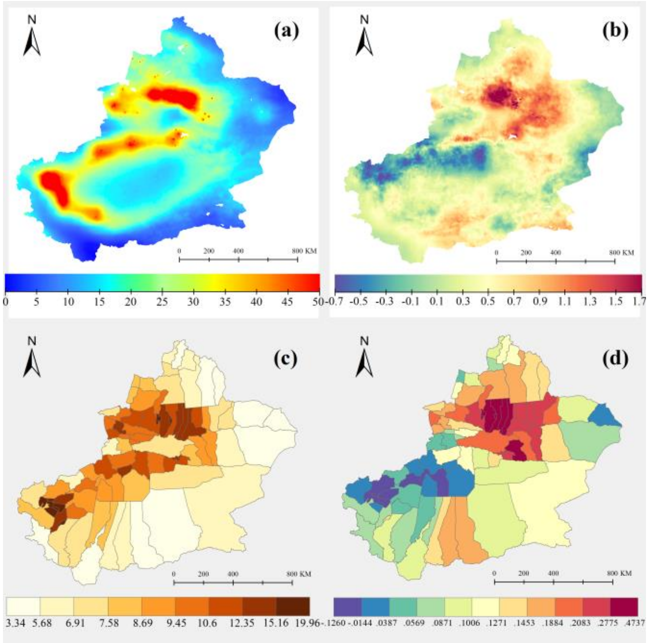

Fig. 1. Spatial distributions of average annual $PM_{2.5}$ (a)(c) concentrations and its interannual trends (b)(d)

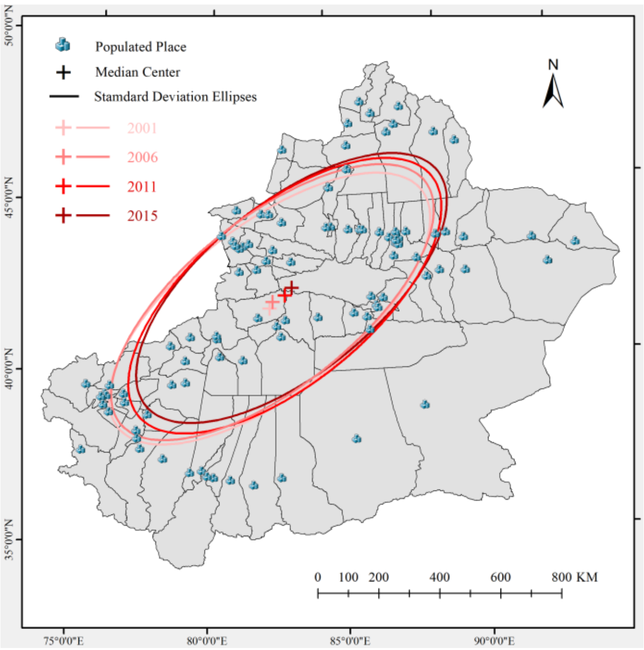

Fig. 2. Spatial changes of the median center and standard deviation ellipses of $PM_{2.5}$ concentrations

As shown in Figure 2, there are 85 county and 106 populated places (more than 200 persons per square kilometers) in Xinjiang. Figure 3 showed the global Moran's I of $PM_{2.5}$ concentrations with maximum value of 0.5733 and minimum 0.4719, which are all positive and significant ($p<0.01$). Most of dots concentrated in the first and third quadrants, meaning that most of country shows the positive spatial autocorrelations of $PM_{2.5}$ concentrations. Similarity, LISA map showed that high $PM_{2.5}$ concentrations cluster in the northern slope of Tianshan Mountain and western Tarim basin and a low $PM_{2.5}$ concentrations cluster in the southern and eastern of Xinjiang.

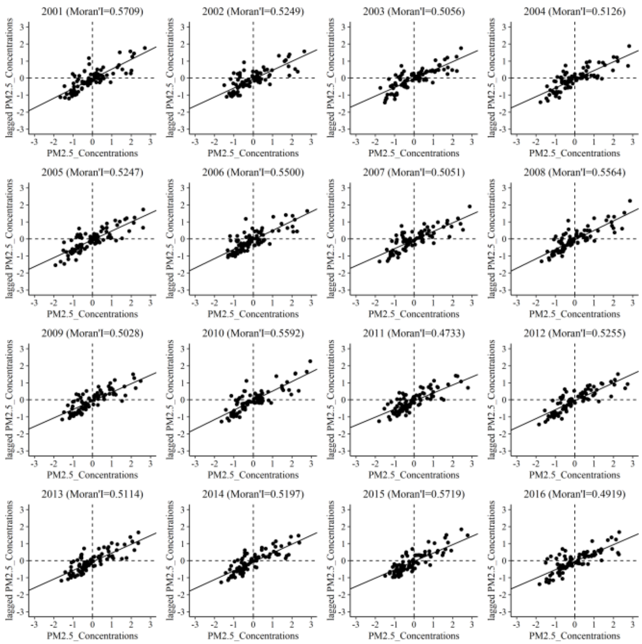

Fig. 3. Global Moran's I scatterplots of $PM_{2.5}$ concentrations (2001-2016)

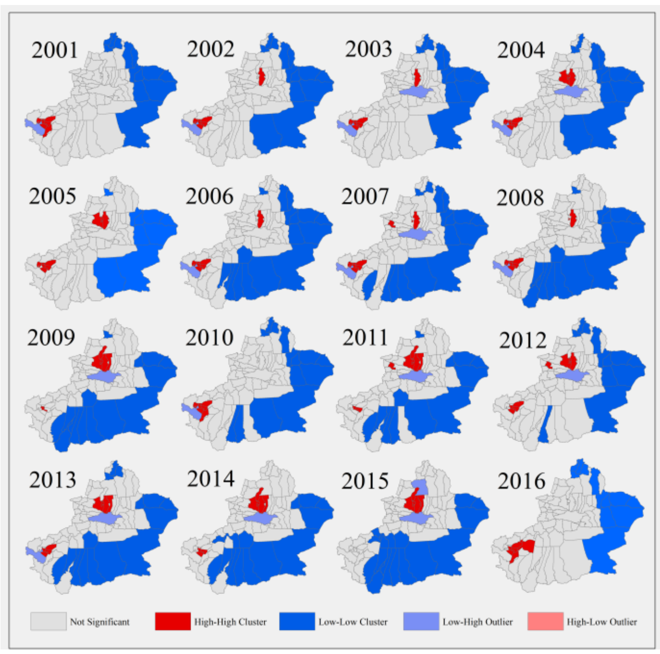

Fig. 4. Spatial agglomeration diagram (LISA map) of $PM_{2.5}$ concentrations (2001-2016)

3.2 The effect of socio-economic factors on $PM_{2.5}$ from the prospective of county scale

Due to the input variable of the GeoDetector model must be the categorial variable, here we used the Quantile method as the discretization method to transform the numerical variables into categorial variables (Fig.5). The dependent variable are as follows, GDP density (GDP_D), GDP per capita (GDPPC), INGDP density (INGDP_D), INGDP per capita (INGDPPC), POP, POP density (POP_D), Road_L, Road network density (Road_D), River network density (River_D). The factor detector show population density was the dominant factor on the distribution of $PM_{2.5}$ concentrations (q=0.550), followed by River network density (q=0.423), GDP density (q=0.413), INGDP density (q=0.212), GDP per capita (q=0.161). The results of other factors were not significant at the 0.05 level. According to the risk detector module of the GeoDetector model, the average $PM_{2.5}$ concentrations in each stratum of different factors were calculated (Fig.6b). As shown in Figure 6c, the interaction between any two factors can enhance their explanatory power for the spatial distribution in $PM_{2.5}$ concentrations. The dominant interactions between GDPPC and Road_D show the highest q values (q=0.785), and it belonged to the bivariate enhancement interaction ($q(X1 \cap X2) > q(X1) + q(X2)$). The ecological detector result showed that the POP_D has a significantly stronger effect on $PM_{2.5}$ than other factors except GDP_D (Fig.6d).

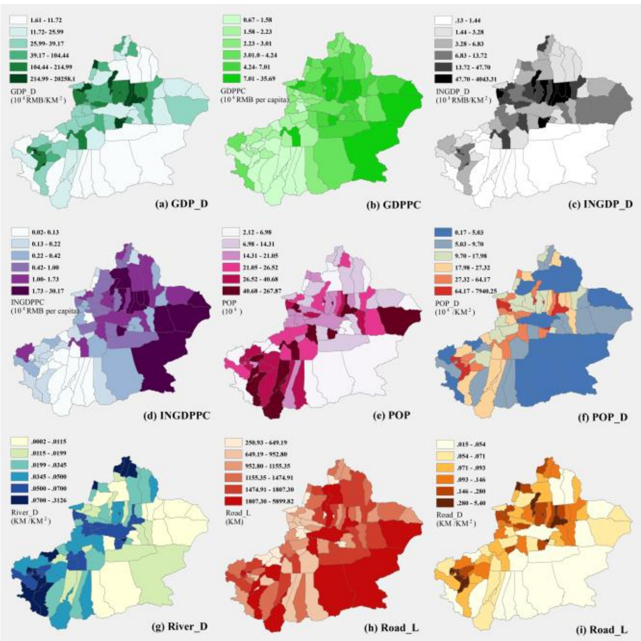

Fig. 5. Spatial distributions of discretization result for 9 continuous variables based on Quantile method

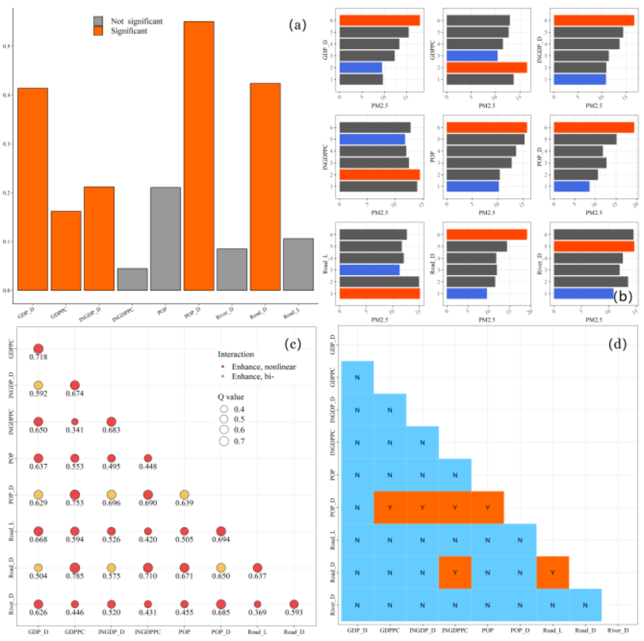

Fig. 6. The result of GeoDetector model: Factor detector(a), Risk detector(b), Interaction detector(c), Ecological detector(d)

3.3 The interannual variation of potential driving factors for $PM_{2.5}$ concentrations

Due to the lack of continuous and reliable long time series of socio-economic data, night time stable light with high spatial resolution data was used to instead of these in this study. However, National Geophysical Data Center stopped producing monthly composites of DMSP_OLS data after February 2013, while NPP/VIIRS, which was supplied in April 2012, is a follow-up to DMSP_OLS. In this study, an exponential model was used to fit the two data sources which were desaturated and resampled to 1km. The Mean Absolute Error (MAE), Root Mean Square Error (RMSE), R2 and the Pearson Correlation Coefficient R between two data sources were calculated to evaluate model fitting effects (Fig.7b), and a good fit was shown. The more intuitive night light image fitting results are shown in Figure 7cd.

As descried in the section 3.1, $PM_{2.5}$ concentrations gradually changed in the terms of the spatiotemporal distribution. In this research, the q-value was used to describe the interannual variation of $PM_{2.5}$ potential driving factors, during the study period of 2001-2016. As shown in Figue.8, the explanatory power of population density decreased significantly. Conversely, DEM, NSL, LCT and NDVI show the increased trend on the driving forces of $PM_{2.5}$ concentrations.

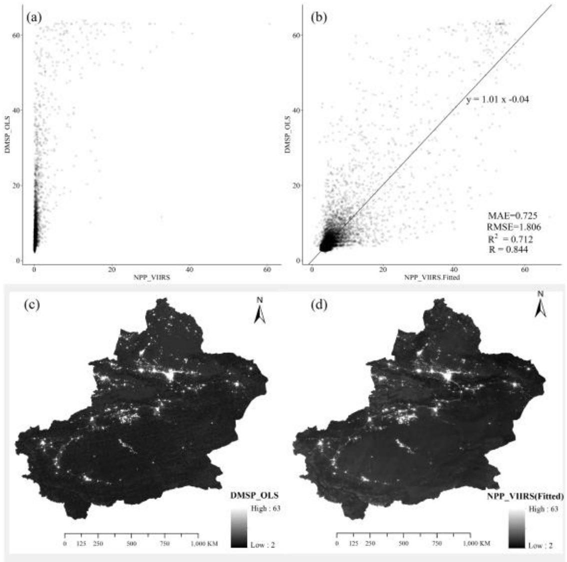

Fig. 7. The relationship between DMSP_OLS NSL and before and after NPP_VIIRS NSL Fitted in 2013 (a)(b), and the spatial distribution of DMSP_OLS NSL(c) and NPP_VIIRS NSL Fitted in 2013(d).

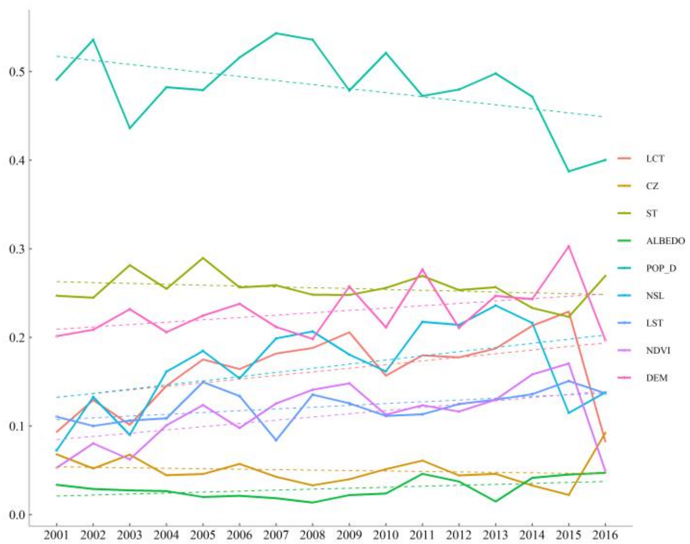

Fig. 8. The q value of each driving factors and their tendency (2001-2016).

4 Discussion and conclusion

Given the paucity of comprehensive studies about the spatiotemporal variations in $PM_{2.5}$ concentrations and its determinants in the whole Xinjiang, we have systematically analysed spatiotemporal characteristics of $PM_{2.5}$ concentrations and its natural social economy determinants. Xinjiang is situated in the northwest of China and the center of Eurasian continents. The fundamental characteristics of oasis-desert ecological environment in Xinjiang determine the unique spatiotemporal aggregation pattern and environment driven mechanism of $PM_{2.5}$ concentrations. The spatial distribution of $PM_{2.5}$ concentrations show that the north slope of Tianshan mountain and the western Tarim desert have the highest $PM_{2.5}$ concentrations. Meanwhile, we found that there are global and local spatial autocorrelation in the study area and High-High clusters are mainly distributed in the two areas we mentioned above. From 2001 to 2015, the mean center of $PM_{2.5}$ concentrations in Xinjiang showed a notably moved to the northeast by reason of the rise of $PM_{2.5}$ concentrations in the north slope of Tianshan mountain and the lower of $PM_{2.5}$ concentrations in the northwest of the western Tarim desert. By the means of GeoDetector model, we found that population density was still the greatest power of determinant on $PM_{2.5}$ concentrations. Moreover, GDP per capita and road network density show the strongest interaction effects in 2016. Due to the Rapid urbanization and the development of heavy industry, the impact of population density showed a fall trend. Indeed, some factor like NSL which can represent the urban size and the level of economic activity, has the significant upward trend along the study period. Furthermore, the explanatory power of DEM NDVI, LCT increased by a significant trend. With the increase of the area of artificial oasis in the edge of Tarim desert for the last 16 years, this improves the ecological environment of the desert edge cities and increases the absorption capacity of farmland for $PM_{2.5}$.

As we all known, dust play a vital role in some region of Xinjiang[23,24]. The raw data of $PM_{2.5}$ were estimated with dust removed by AOD product. The dust and interactions between dust and other factors was not be considered in this study. The second limitation of this study is that climate factors are not considered, which also creates some uncertainty about the results.

References

1. Han, X.; Liu, Y.; Gao, H.; Ma, J.; Mao, X.; Wang, Y.; Ma, X. Forecasting PM 2.5 induced male lung cancer morbidity in China using satellite retrieved PM 2.5 and spatial analysis. *Science of the Total Environment* **2017**, *s 607–608*, 1009-1017.

2. Hoek; Gerard; Beelen; Rob; Krishnan; Ranjini, M.; Kaufman; Joel, D.; Peters; Annette. Long-term air pollution exposure and cardio- respiratory mortality: a;review. *Environ Health* **2013**, *12*, 43.

3. Zhu, W.; Luo, L.; Cheng, Z.; Yan, N.; Lou, S.; Ma, Y. Characteristics and contributions of biogenic secondary organic aerosol tracers to PM2.5 in Shanghai, China. *Atmospheric Pollution Research* **2018**, *9*, 179-188, doi:https://doi.org/10.1016/j.apr.2017.09.001.

4. Ping, S.; Xin, J.; An, J.; Kong, L.; Wang, B.; Wang, J.; Wang, Y.; Dan, W. The empirical relationship between PM 2.5 and AOD in Nanjing of the Yangtze River Delta. *Atmospheric Pollution Research* **2016**, *8*, 233-243.

5. Li, X.; Zhang, Q.; Zhang, Y.; Zheng, B.; Wang, K.; Chen, Y.; Wallington, T.J.; Han, W.; Shen, W.; Zhang, X. Source contributions of urban PM 2.5 in the Beijing–Tianjin–Hebei region: Changes between 2006 and 2013 and relative impacts of emissions and meteorology. *Atmospheric Environment* **2015**, *123*, 229-239.

6. Turap, Y.; Talifu, D.; Wang, X.; Abulizi, A.; Maihemuti, M.; Tursun, Y.; Ding, X.; Aierken, T.; Rekefu, S. Temporal distribution and source apportionment of PM2.5 chemical composition in Xinjiang, NW-China. *Atmospheric Research* **2019**, *218*, 257-268, doi:https://doi.org/10.1016/j.atmosres.2018.12.010.

7. Tai, A.P.K.; Mickley, L.J.; Jacob, D.J. Correlations between fine particulate matter (PM2.5) and meteorological variables in the United States: Implications for the sensitivity of PM2.5 to climate change. *Atmospheric Environment* **2010**, *44*, 3976-3984, doi:https://doi.org/10.1016/j.atmosenv.2010.06.060.

8. Sæbø, A.; Popek, R.; Nawrot, B.; Hanslin, H.M.; Gawronska, H.; Gawronski, S.W. Plant species differences in particulate matter accumulation on leaf surfaces.

Science of The Total Environment **2012**, *427-428*, 347-354, doi:https://doi.org/10.1016/j.scitotenv.2012.03.084.

9. Van, D.A.; Martin, R.V.; Brauer, M.; Hsu, N.C.; Kahn, R.A.; Levy, R.C.; Lyapustin, A.; Sayer, A.M.; Winker, D.M. Global Estimates of Fine Particulate Matter using a Combined Geophysical-Statistical Method with Information from Satellites, Models, and Monitors. *Environmental Science & Technology* **2016**, *50*, 3762.

10. Friedl, M.; Sulla-Menashe, D. MCD12Q1 MODIS/Terra+ Aqua land cover type yearly L3 global 500m SIN grid V006 [data set]. *NASA EOSDIS Land Processes DAAC. Doi* **2015**, *10*.

11. Schaaf, C.; Wang, Z. MCD43A3 MODIS/Terra+ Aqua BRDF/Albedo Daily L3 Global—500 m V006. *NASA EOSDIS Land Processes DAAC* **2015**, *10*.

12. Wan, Z.; Hook, S.; Hulley, G. MOD11A2 MODIS/Terra land surface temperature/emissivity 8-day L3 global 1km SIN grid V006. *NASA EOSDIS Land Processes DAAC* **2015**, *10*.

13. Didan, K. MOD13Q1 MODIS/Terra vegetation indices 16-day L3 global 250m SIN grid V006. *NASA EOSDIS Land Processes DAAC* **2015**.

14. Shi, K.; Huang, C.; Yu, B.; Yin, B.; Huang, Y.; Wu, J. Evaluation of NPP-VIIRS night-time light composite data for extracting built-up urban areas. *Remote Sensing Letters* **2014**, *5*, 358-366.

15. Elvidge, C.D.; Baugh, K.E.; Kihn, E.A.; Kroehl, H.W.; Davis, E.R. Mapping city lights with nighttime data from the DMSP Operational Linescan System. *Photogrammetric Engineering and Remote Sensing* **1997**, *63*, 727-734.

16. Jarvis, A.; Reuter, H.I.; Nelson, A.; Guevara, E. Hole-filled SRTM for the globe Version 4. *available from the CGIAR-CSI SRTM 90m Database (http://srtm. csi. cgiar. org)* **2008**, *15*, 25-54.

17. Beck, H.E.; Zimmermann, N.E.; McVicar, T.R.; Vergopolan, N.; Berg, A.; Wood, E.F. Present and future Köppen-Geiger climate classification maps at 1-km resolution. *Scientific Data* **2018**, *5*, 180214, doi:10.1038/sdata.2018.214.

18. Tatem, A.J. WorldPop, open data for spatial demography. *Scientific data* **2017**, *4*.

19. Jian, P.; Sha, C.; Lü, H.; Liu, Y.; Wu, J. Spatiotemporal patterns of remotely sensed PM 2.5 concentration in China from 1999 to 2011. *Remote Sensing of Environment* **2016**, *174*, 109-121.

20. Moran, P.A.P. Notes on Continuous Stochastic Phenomena. *Biometrika* **1950**, *37*, 17-23, doi:10.2307/2332142.

21. Anselin, L. Local Indicators of Spatial Association—LISA. *Geographical Analysis* **1995**, *27*, 93-115, doi:10.1111/j.1538-4632.1995.tb00338.x.

22. Wang, J.F.; Li, X.H.; Christakos, G.; Liao, Y.L.; Zhang, T.; Gu, X.; Zheng, X.Y. Geographical Detectors-Based Health Risk Assessment and its Application in the Neural Tube Defects Study of the Heshun Region, China. *International Journal of Geographical Information Science* **2010**, *24*, 107-127.

23. Liu, D.; Abuduwaili, J.; Lei, J.; Wu, G. Deposition rate and chemical composition of the aeolian dust from a bare saline playa, Ebinur Lake, Xinjiang, China. *Water, Air, & Soil Pollution* **2011**, *218*, 175-184.

24. Ge, Y.; Abuduwaili, J.; Ma, L.; Wu, N.; Liu, D. Potential transport pathways of dust emanating from the playa of Ebinur Lake, Xinjiang, in arid northwest China. *Atmospheric Research* **2016**, *178-179*, 196-206, doi:https://doi.org/10.1016/j.atmosres.2016.04.002.